Polymorphic phase transformation of Degussa P25 TiO$_2$ by the chelation of diaminopyridine on TiO$_6^{2-}$ octahedron: Correlation of anatase to rutile phase ratio on the photocatalytic activity

K. Eraiah Rajashekhar, L. Gomathi Devi*

Department of Post Graduate Studies in Chemistry, Bangalore University, Central College City Campus, Dr. Ambedkar street, Bangalore 560001, India

ABSTRACT

A series of nitrogen-doped Degussa P25 photocatalysts were synthesized successfully by grinding and calcination method using 2,6-diaminopyridine (DAP) as a nitrogen precursor. The prepared samples were characterized by various analytical methods. The phase contents of anatase and rutile in the Degussa P25 powders have been altered by simply changing the proportion of DAP. A mechanism involving chelated DAP molecule on TiO$_6^{2-}$ octahedron is discussed. The enhanced activity is attributed to synergistic effect in the two phase solid material. Due to the low activation barrier, the effective inter particle electron transfer between the two polymorphs is quite efficient only when they are in close proximity with similar crystallite sizes. The transfer of electrons from the rutile phase to lattice/electron trapping sites of anatase and also to the Ti^{3+}-V$_o$ defect level created by the dopant favors effective charge separation and enhance the photocatalytic activity under solar illumination.

© 2013 Elsevier B.V. All rights reserved.

1. Introduction

The Degussa P25 TiO$_2$ (P25) is a well known commercial material containing anatase and rutile phases in the ratio of ∼3:1[1]. It is widely used in various technological application such as solar energy storage cells [2,3], catalyst in the synthesis of organic compounds [4,5], degradation of organic contaminants in gaseous phase and aqueous systems [6,7], degradation of volatile acetone as an indoor air pollutant into CO$_2$ and water [8], abatement of the *E. coli* bacteria under solar simulated light [9]. P25 shows excellent photocatalytic activity because of the adsorptive affinity of organic compounds on the surface of anatase whose percentage is higher than that of rutile phase. In addition anatase exhibits lower rates of recombination in comparison to rutile due to its 10-fold higher rate of hole trapping capacity [10,11]. However, the inherent limitation of P25 is the large band gap (3.2 eV), which hinders it being active in the visible region (λ > 400 nm). Many approaches have been made to improve the visible light response of P25. Doping with various nonmetal ions like N, C, S etc., is one of the effective method for preparing visible light active photocatalyst. There are three possible ways to incorporate nitrogen atoms in to the TiO$_2$ lattice: (i) replacement of lattice oxygen by an N atom, (ii) replacement of Ti atom by an N atom (These two mechanisms imply the rapture of Ti—O bonds that must be replaced either by Ti—N or by N—O bonds),

(iii) incorporation of N at an interstitial position which may occur without inducing too much strain in the structure, but it is less probable due to the higher size of N atom. It has been reported that the milling atmospheres with different oxygen partial pressures had an influence on the transformation kinetics of anatase to rutile, when the nanocrystalline TiO$_2$ powders were milled in oxygen, air and nitrogen atmospheres respectively [12,13]. Yin et al. reported phase transformation of anatase to rutile using P25 titania by ball milling the powder with hexamethylenetetramine as a nitrogen precursors [14]. Kang et al. have used NH$_3$ as nitrogen source and they have observed that grinding the samples in the presence of gaseous ammonia increases the specific surface area, with in an increase in the grinding time period [15]. However comparison of photocatalytic activity and determining the factors which influence their activity is greatly restricted. This is because the rutile is prepared as thermally stable phase and usually possesses much smaller surface area and larger crystallite size than anatase TiO$_2$. In fact, some researchers have demonstrated that rutile titania with smaller crystalline size and with larger surface area possess high photocatalytic activity [16–20]. Liu et al. also reported that the iodine doped TiO$_2$ with a two phase solid material shows much better activity than the anatase TiO$_2$, when the crystal sizes of rutile and anatase phase were comparable [21]. In the present work, diaminopyridine (DAP) was used as the nitrogen precursor. The phase contents of anatase and rutile in the P25 powders have got altered by simply changing the proportion of DAP and the performance of the catalyst was tested for the photodegradation of Methylene Blue (MB).

* Corresponding author. Tel.: +91 80 22961336; fax: +91 80 22961331.
  E-mail address: gomatidevi_naik@yahoo.co.in (L.G. Devi).

2. Experimental method

2.1. Materials

Degussa P25 TiO_2 was used as the starting material to prepare nitrogen doped titania. 2,6-Diaminopyridine ($C_5H_7N_3$) is obtained from Merck chemicals Ltd. MB is a cationic dye which was obtained from Aldrich. The molecular formula of MB is $C_{16}H_{18}ClN_3S$ and the molecular weight is 319.85. Double distilled water was used in all the experiments.

2.2. Catalyst preparation

For the preparation of non metal ion doped TiO_2, a known concentration of nonmetal ion solution was added to the calaculated amount of TiO_2 to get the desired dopant concentration in the range of 0.04–0.2 wt.%. For example the preparation of 0.04 wt.% N doped P25 (NTP25-04), 0.1039 g of DAP (0.04 g of N) was dissolved in 100 ml double distilled water. 1 ml of this solution (contains 0.001039 g of DAP or more precisely it contains 0.0004 g of N) is added to the 1 g of P25 to get NTP25-04. The mixture was ground in a pestle and mortar and oven dried at 120 °C for one hour. The process of grinding is repeated for four times and the powder is finally calcined at 550 °C for 5 h. Similar stoichiometric volume of DAP solution (solution A) was added to the calculated amount of P25 to get the dopant concentration in the range of 0.1, 0.15 and 0.2 wt.%, which are abbreviated as NTP25-10, NTP25-15 and NTP25-20 respectively.

2.3. Characterization of the catalyst

The Powder X-ray diffraction (PXRD) patterns of the samples were obtained using Philips pw/1050/70/76. The diffractometer was operated at 30 kV and 20 mA. Cu Kα was used as a source with nickel filter at a scan rate of 2°/min. The average crystallite size (D) was calculated (at a scan rate of ½°/min) in accordance with Scherrer's formula $D = k\lambda/\beta\cos\theta$, where k is the constant (shape factor, ~0.9), λ is the X-ray wavelength (0.15418 nm), β is the full width at half maximum (FWHM) of the diffraction line and θ is the diffraction angle. The values of β and θ are taken for crystal plane (1 0 1) of anatase phase and (1 1 0) for rutile phase. Fourier transfer infra red spectra (FT-IR) were recorded using Nicolet Impact 400 D FTIR spectrometer with potassium bromide as the reference. X-ray photoelectron spectra (XPS) were recorded with ESCA-3 Mark II spectrometer (VG Scientific Ltd., U.K.) using Al Kα radiation (1486.6 eV). XPS experiments were performed in a standard UHV chamber (base pressure 3×10^{-9} Torr) equipped with a 100 mm hemispherical electron analyzer (Scienta, SES 100). The spectrometer was calibrated by setting the binding energies of Au $4f_{7/2}$ and Cu $2p_{3/2}$ to 84.0 and 932.7 eV respectively. The binding energy for the samples is normalized with reference to the C 1s peak at 284.6 eV resulting from the adsorbed hydrocarbon fragment. The XPS binding energies were measured with a precision of 0.1 eV. No surface cleaning or ionic etching was performed before the experiment since it may induce some modification or damage to the surface. C 1s line was taken as reference for all the samples. Analysis of XPS spectra was done by peak decomposition procedure by using Gaussian-Lorentzian curve fitting. Photoluminescence (PL) spectra were recorded on a Hitachi F-7000 fluorescence spectrophotometer. The diffuse reflectance spectra (DRS) were obtained with Schimadzu-UV 3101 PC UV-VIS-NIR spectrophotometer, using $BaSO_4$ as the reference sample. Kubelka–Munk plot was used to calculate the band gap energy values. It is a plot of $(1 - R_\infty)^2/2R_\infty$ (relative reflective intensity) versus wavelength, where R_∞ is the ratio of relative reflected intensity of the sample to that of non-absorbing standard ($BaSO_4$). $(1 - R_\infty)^2$ is

the molar absorption coefficient and $2R_\infty$ is the scattering coefficient. Surface morphology was analyzed by JSM840 scanning electron microscope (SEM) operating at 25 kV. A thin layer of gold had been evaporated on the surface of the specimen. The specific surface area and pore volume of the powders were measured by dynamic Brunner–Emmet–Teller (BET) method in which N_2 gas was adsorbed at 77 K using Digisorb 2006 Nova Quanta Chrome Corporation Instrument. The specific surface area was determined by multipoint BET method using the adsorption data in the relative pressure (P/P_o) range of 0.05–0.3. Desorption isotherm were used to determine the pore size distribution, pore volume and pore diameter using the Barret–Joyner–Halender (BJH) method. Prior to the measurements, the catalysts were calcined at 150 °C for 1 h.

2.4. Photocatalytic degradation procedure

Artificial light source of 125 W medium pressure mercury vapor lamp with the photon flux of 8.1 mW/cm² whose wavelength of emission is ~370 nm was used as UV source. All the experiments were carried out in a circular borosilicate glass reactor with exposure surface area of 176 cm². Photocatalysis under solar light was performed between 11 am and 2 pm during the summer season in the months of April–June at Bangalore, India. The latitude and longitude of the place is 12.58N and 77.38E respectively. The average solar intensity was found to be 0.753 kW m^{-2} (using solar radiometer). The intensity of solar light was concentrated by convex lens and the reaction mixture was exposed to this concentrated solar light. In a typical experiment 250 ml solution having 40 mg/L of MB solution along with 400 mg/L of photocatalyst were used. The reaction mixture is stirred vigorously using magnetic stirrer for the entire time span of the experiment. The samples were collected at different time intervals and were subjected to centrifugation followed by the filtration through 0.45 μm Millipore filter to remove the catalyst particles. The residual concentration of the MB was determined by UV–vis spectroscopy in the wavelength range of 190–600 nm.

3. Results and discussions

3.1. Powder X-ray diffraction (PXRD) studies

Fig. 1 shows the PXRD pattern of P25 and NTP25 samples. The anatase phase of titania shows a major peaks at $2\theta = 25°$, 37°, 48°, 55°, 56°, 62°, 71° and 75° and rutile phase shows the major peaks at $2\theta = 28°$, 36°, 42°, and 57°. They are indicated as A and R in the Fig. 1. The rutile mass fraction in the sample was calculated using the Spurr and Meyer's equation [22]:

$$X_R = \left(1 + \frac{0.884 I_A}{I_R}\right)^{-1} \qquad (1)$$

$$X_A = 1 - X_R \qquad (2)$$

X_R and X_A are the mass fraction of rutile and anatase phase contents in the powders. I_A and I_R are the X-ray integrated intensities of the strongest peaks corresponding to the plane 1 0 1(at $2\theta = 25°$) reflection of anatase and the plane 1 1 0 (at $2\theta = 28°$) reflection of rutile. Phase compositions of all the samples are given in the Table 1. The atoms in the defect sites have higher energy than those in the main lattice and can favorably act as nucleation sites for the rutile phase formation at the surface of anatase crystallites. Thus the high concentration of nucleation sites for the polymorphic phase transition from anatase to rutile exists at particle-particle interfaces in comparison to the bulk. This might result in the increase of rutile fraction for NTP25-04. The rutile mass fraction increases with increase in the DAP concentration up to 0.15 wt.%. But further increase in the DAP concentration (0.20 wt.%), the rutile mass
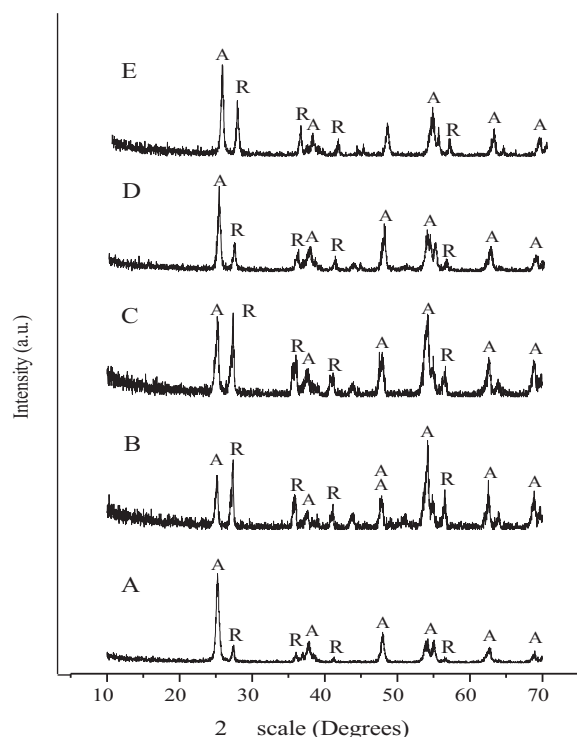
Fig. 1. PXRD patterns of P25 and various NTP25 samples. (A) P25, (B) NTP25-04, (C) NTP25-10, (D) NTP25-15 and (E) NTP25-20 (A: anatase and R: rutile phases).

content decreases. The variation of anatase to rutile phase content ratio versus the nitrogen concentration is given in the supplementary material as S1. Crystallite sizes of doped samples were smaller compared to the undoped sample [23–26]. Parida et al. have also reported similar results for nitrogen doped samples, crystallite size decreases with increase in the urea concentration [26]. Similar results were also reported by Li et al. where nitrogen doped TiO_2 had smaller crystallite size and larger specific surface area with surface oxygen defects produced by nitrogen dopant [27]. The change in the ratio of anatase to rutile mass fraction and the change in the crystallite size confirm the incorporation of nitrogen in the host lattice. The literature data show that the anatase-rutile phase transformation takes place at a temperature of 780 °C for pure titania [24]. The temperature for the transformation can vary from 400 to 1200 °C depending on various factors like: (a) the type and amount of additives. (b) Method of powder preparation and (c) heating atmosphere. These processing variables would significantly change the phase transformation rate and activation energy. This produces a transition temperature either higher or lower than that of pure titania [24].

3.2. UV–vis diffuse reflectance spectral studies

The band gap energies of photocatalysts were calculated using Kubelka–Munk plot of $(1 - R_\infty)^2/2R_\infty$ versus wavelength as shown

Table 1
Summary of the structural data obtained by PXRD patterns of P25 and NTP25 samples.

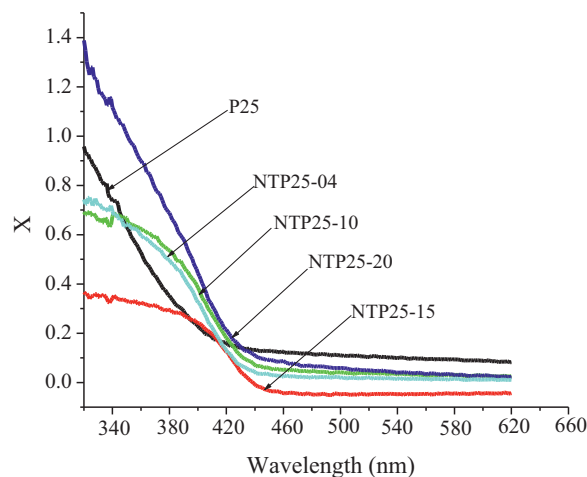| Photocatalysts	Fraction (wt.%)		Crystallite size (nm)	
	A	R	A	R
P25	82	18	25.6	85.6
NP25-04	46	54	50.1	88.1
NP25-10	51	49	51.1	58.7
NP25-15	77	23	42.4	56.9
NP25-20	65	35	43.8	58.7

Fig. 2. Kubelka–Munk plot for doped and undoped P25.

in Fig. 2 and corresponding band gap energy values are given in the Table 2. The band gap energy values shifts to longer wavelength on nitrogen incorporation. The extent of red shift in the band gap was higher for NTP25-15 sample compared to other doped samples. The shift in the band gap to the visible region for the doped samples arises due to the electronic transition between the defect levels to the band gap energy states of P25. The doping of heteroatom results in the formation of additional energy level above the valence band of P25. It is well known that valence and conduction band of P25 are mainly formed due to the major contribution by the completely filled O 2p orbital and the empty Ti 3d orbital respectively. The 2p orbital of the doped nitrogen atom significantly interacts with the 2p orbital of the oxygen.

3.3. XPS analysis

XPS spectra of P25 and NTP25 samples are shown in supporting materials S2. A broad N 1s peak observed at 396–399 eV confirms the incorporation of nitrogen in the TiO_2 lattice. The peak at a binding energy of 396.6 eV can be assigned to the substitutionally incorporated nitrogen in the TiO_2 lattice [28,29,23]. The XPS spectrum of Ti $2p_{3/2}$ shows a peak at 458.6 eV and 457.9 eV for P25 and NTP25 samples. The peak corresponding to Ti $2p_{3/2}$ shows a shift in the binding energies with increase in the nitrogen content. O 1s peaks were found at ~529 eV in N doped samples which could be assigned to the lattice oxygen of TiO_2. Similar shift was also observed in O 1s peak with increase in the dopant content. The shift of both O 1s, Ti $2p_{3/2}$ in the binding energy indicates the increase of the electron densities on the Ti atom suggesting that some Ti^{3+} species may exist in all the four samples [30]. Miao et al. and Jagadale et al. have also assigned these shifted peaks to $TiO_{2-x}N_x$ [31]. These results provide strong evidence for the substitutional incorporation of nitrogen in the TiO_2 lattice. The observed shift in the binding energy is due to the surface strain and lattice distortion induced by the incorporated nitrogen dopant. Nitrogen contents were measured using the method of the relative sensitivity of detection of the elements [32]. $n_1/n_2 = (I_1 S_2)/(I_2 S_1)$, where n_1 and n_2 are the concentrations of nitrogen and oxygen in the sample, I_1 and I_2 are the corresponding intensities, S_1 and S_2 are the relative sensitivity values (0.42 for N 1s and 0.52 for O 1s) obtained by using C 1s line as the standard. The nitrogen content in the various doped catalysts are obtained from the XPS data and they are listed in the Table 2.

Table 2
Nitrogen content (wt.%) from XPS studies, BET surface area, pore size, absorption threshold, band gap energies of P25 and NTP25 samples.

Sample	Nitrogen content (atom.%)	BET surface area (m²/g)	Porosity (cm³/g)	Absorption threshold (nm)	Band gap energy (eV)
P25	–	50	0.25	380	3.26
NP25-04	0.036	58	0.28	426	2.91
NP25-10	0.061	59	0.31	436	2.84
NP25-15	0.119	66	0.34	454	2.72
NP25-20	0.165	62	0.33	444	2.79

3.4. FTIR studies

Fig. 3 shows the infrared spectra of P25 and NTP25 samples. The peaks at ~3420 and ~1630 cm^{-1} are assigned to the stretching and bending vibrations of the hydroxyl groups (O—H). The peaks at ~2920 and ~2840 cm^{-1} were attributed to the Ti—OH bond [33–36]. The broad absorption band in the region 500–800 cm^{-1} is assigned to the stretching vibration of Ti—O and Ti—O—Ti bonds [33]. A new absorption peak is observed for NTP25 samples at ~1060, ~1120 and ~1160 cm^{-1} can be assigned to the N—Ti—O stretching vibration [33]. The peak observed at 1400 cm^{-1} for nitrogen doped samples can be assigned to the N—H bending vibration.

FTIR spectra of the samples DP25, DAP, DP25 + DAP before and after calcinations are shown in Fig. 4. The bands observed around 1119, 1170 cm^{-1} for P25 + DAP (before calcination) and 1170 cm^{-1} for P25 + DAP (after calcination) should be the characteristic band of the monodentately bonded nitrogen species on the surface of P25. The peaks at 1590 and 1450 cm^{-1} are particularly diagnostic of aromatic structure observed in DAP, P25 + DAP (before calcinations) samples. These aromatic C—C skeletal in plane vibrations are not shown by the P25 + DAP samples after calcinations implying the destruction of aromaticity. The peaks observed in the spectra of DAP at 1350–1260 cm^{-1} can be assigned to C—N bond (nitrogen attached to the aromatic carbon). These peaks completely disappear after calcination.
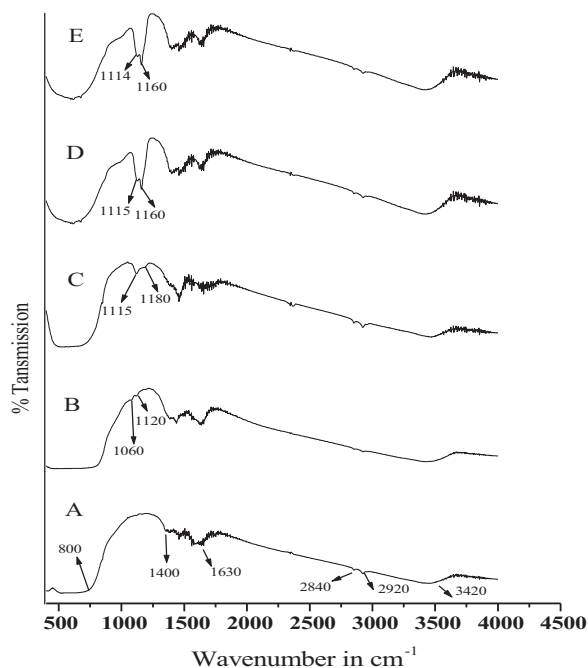
3.5. Surface morphology and surface area studies

Fig. 5 shows SEM micrographs of P25 and NTP25 samples. The NTP25-04, NTP25-10, NTP25-15 (B–D in Fig. 5) shows the layered structure due the high rutile concentration. This plane structure is lost for NTP25-20 (E in Fig. 5). The retention of the layered structure implies the ionic bonds between the O and N in TiO$_2$ lattice.

This micrograph with higher magnification is shown in Fig. 5(F).

Analysis from BET method shows that specific surface area of the doped samples increases from 50.1 (P25) to 66.23 m²/g (NTP25-15) as shown in the Table 2. With further increase in the dopant concentration, the specific surface area decreases for NTP25-20.

3.6. Fluorescence studies

The decay profiles of the prepared samples were investigated by measuring the fluorescence lifetime. The fluorescence decay profiles of all the photocatalysts under the excitation wavelength of 380 nm are shown in the Fig. 6. These decay profiles were measured using the extended exponential function [37]:

$$I = I_0 t^{\beta-1} \exp\left[-\left(\frac{t}{\tau}\right)^{\beta}\right] \qquad (3)$$

where τ is the lifetime and β is the shape factor. This exponential function has been widely used for the analysis of charge carrier dynamics in semiconductors [38]. Decay profiles shows quit good fitting for all doped samples and it is obtained using the above equation. The existence of carrier trapping sites at different energy levels, leads to a distribution of carrier transport rates. This equation can be used to calculate the lifetime of the charge carriers in the respective catalysts and the results are given in Table 3. There was a systematic decrease in the intensity of the decay
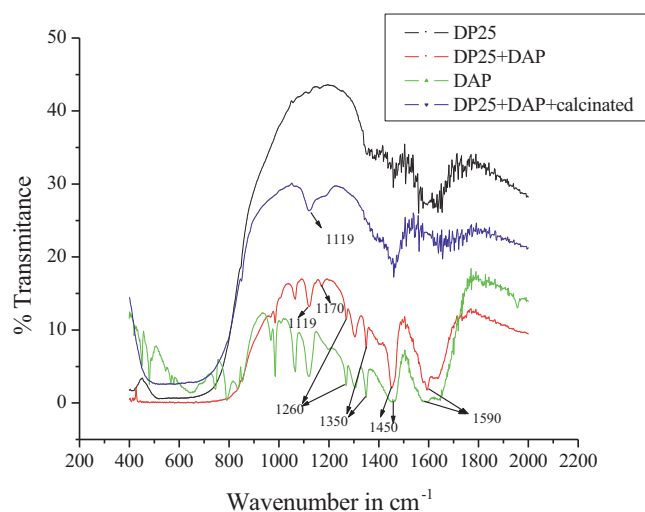

Fig. 3. FTIR spectra of P25 and NTP25 samples. (A) P25, (B) NTP25-04, (C) NTP25-10, (D) NTP25-15 and (E) NTP25-20.

Fig. 4. FTIR spectra of P25, DAP, P25 + DAP (before calcination) and P25 + DAP (after calcination) samples in the spectral region of 200–2200 cm^{-1}. (For interpretation of the references to color in figure legend, the reader is referred to the web version of the article.)
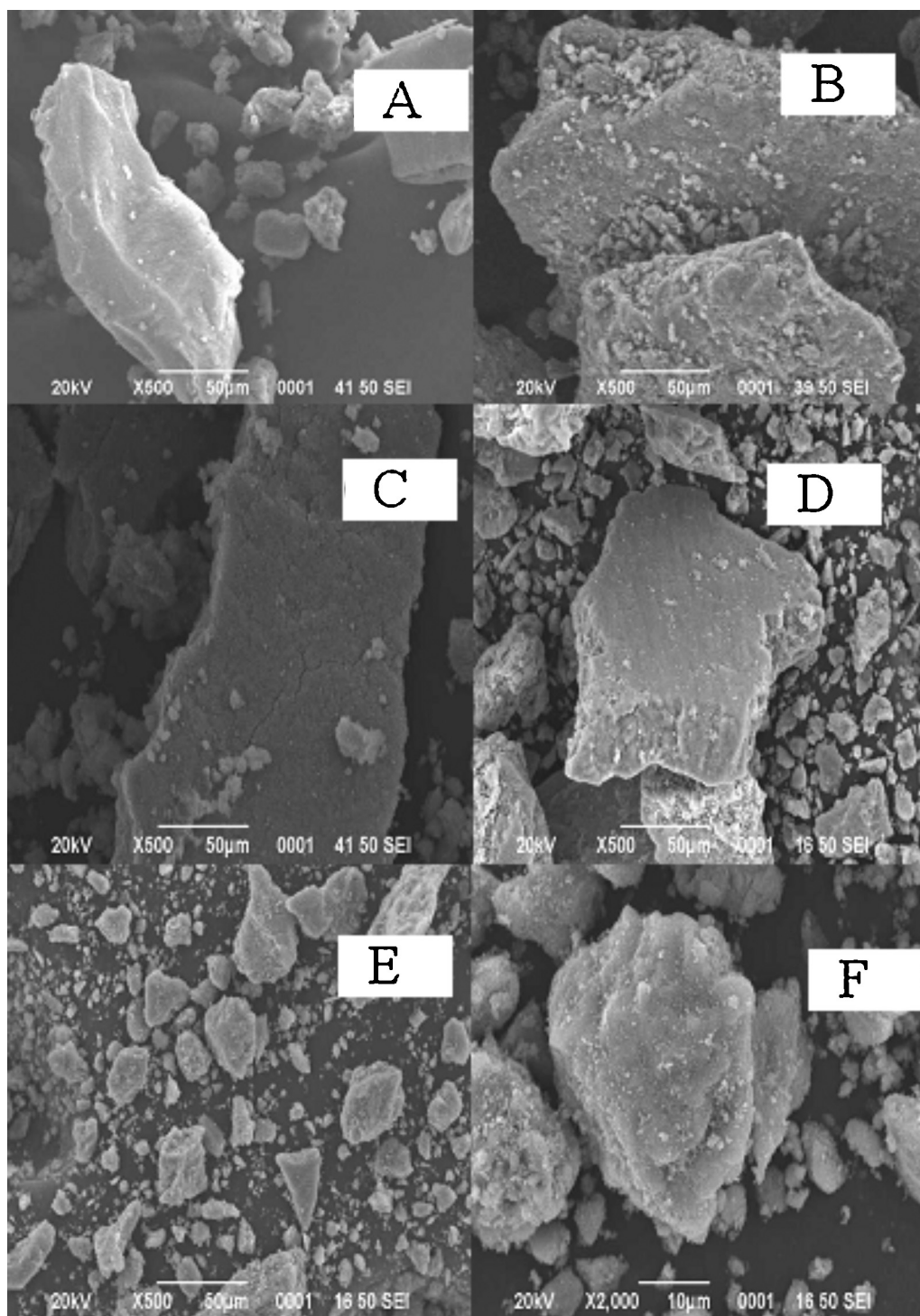
Fig. 5. SEM micrographs of (A) P25, (B) NTP25-04, (C) NTP25-10, (D) NTP25-15, (E) NTP25-20 and (F) NTP25-20 (higher magnification).

Table 3
Fluorescence excitation wavelength, emission lifetime of fluorescence decay profile, apparent first-order rate constant (k_{app}) and percentage degradation of MB under 5 h of UV irradiation and 1.5 h of solar irradiation for the experimental conditions of [MB] = 40 mg/L, [photocatalyst] = 400 mg/L and the reaction solution volume = 250 ml.

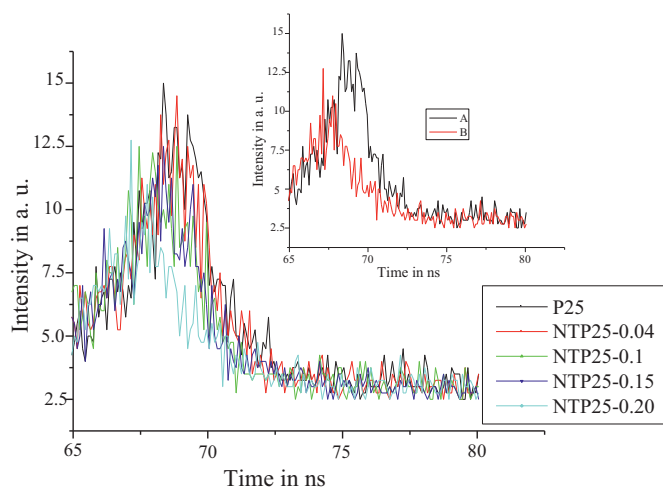| Photocatalyst	Measured excitation wavelength, nm	Lifetime (ns)	k_{app} ($\times 10^{-2}$ min^{-1})		Percentage of degradation	
			UV	Solar	UV	Solar
P25	380	2.15	0.15	0.12	62	20
NTP25-04	380	2.46	0.21	0.45	68	60
NTP25-10	380	2.22	0.26	0.49	84	71
NTP25-15	380, 290	2.12, 1.87	0.28	1.24	100	100
NTP25-20	380	2.15	0.22	0.54	75	77

Fig. 6. Fluorescence decay profiles of P25 and NTP25 samples at excitation wavelength of 380 nm. The inset of the fig shows the fluorescence decay profiles of NTP25-15 photocatalyst under different excitation wavelengths: (A) 290 and (B) 380 nm.

profile with increasing dopant concentration as shown in Fig. 6. The charge carrier recombination reactions are reduced for the doped photocatalyst. The in set of Fig. 6 shows that the lifetime of NTP25-15 is dependent on the excitation wavelength. The decay profile is considered to be mainly determined by the recombination of photogenerated charge carrier [37,39].

3.7. Proposed mechanism for the change in the ratio of anatase to rutile phase contents in P25

DAP (φ-$(NH_2)_2$ where φ is pyridine moiety) molecule acts as a Lewis base. Grinding TiO_2 in presence of DAP accelerate the phase transformation process. This may be due to the interaction of DAP molecule acting as Lewis base on the fresh surface of TiO_2 at Ti^{4+} lattice sites (which acts as Lewis acid sites). Titanium ion first increases its coordination by using its vacant d orbitals to accept the nitrogen electron pairs from nucleophilic ligands such as $-NH$ group of DAP. TiO_2 crystal structures consist of TiO_6^{2-} octahedron, which share edges and corners in different manners that result in the formation of different crystal phases.

Octahedron in anatase share four edges and are arranged in zigzag chains along the [2 2 1] plane, while rutile octahedron share only two edges and form linear chains parallel to the [0 0 1] plane [40–43]. The mechanism of formation of anatase and rutile phases in the presence of DAP is proposed in Scheme 1. The placement of the third octahedron plays a very crucial role in the determination of anatase and rutile phase contents (Scheme 1A) [40]. The presence of DAP would influence the orientation of the third octahedron.

In the beginning at lower DAP concentration, DAP molecule would interact with octahedral hydroxyls by static electricity and formation of rutile nucleation is more favored (Scheme 1B). These results were substantiated by the IR spectroscopic techniques (confirmed from the presence of IR-peak $\sim$1119 cm^{-1} for monodentately bonded nitrogen of DAP on P25 sample after calcination as shown in the Fig. 5). But at higher concentrations of DAP, steric effect plays a major role, the third octahedron would polycondense along the converse direction in order to decrease the repulsion. This decreases the rutile content at higher DAP concentration (Scheme 1C). It has been reported that the presence of nucleophilic ligand accelerates the growth of anatase phase in TiO_2 lattice [41]. Therefore it can be concluded that different concentrations of DAP can alter the anatase to rutile phase ratio in DP25 sample.
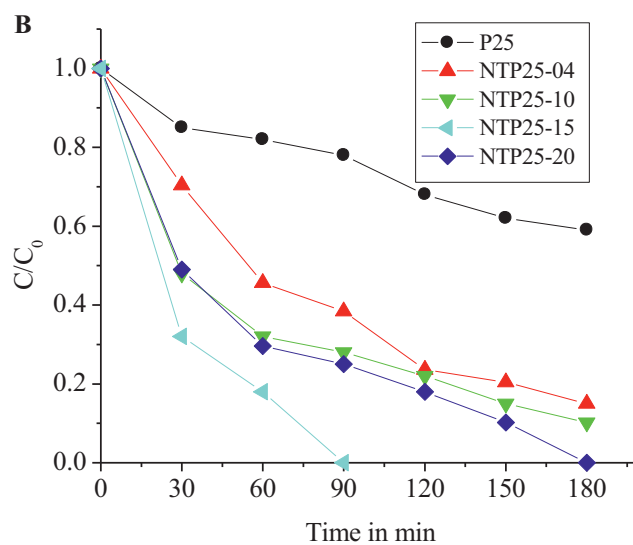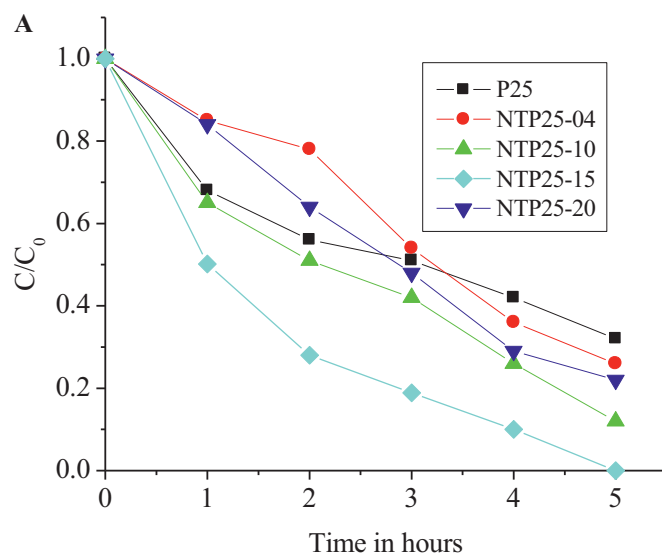

Fig. 7. Plot of C/C_0 versus time (A) under 5 h of UV irradiation and 1.5 h (B) solar irradiation for the degradation of MB using various phtocatalysts [under the experimental conditions of [MB] = 40 mg/L, [photocatalyst] = 400 mg/L].

### 3.8. Correlation of anatase:rutile phase ratio on the photocatalytic activity

The plot of C/C_0 (C_0 is the initial concentration and C is the residual concentration at any given time interval) versus time using different photocatalyst for the degradation of MB under UV/solar irradiation are shown in Fig. 7 and the corresponding rate constant and percentage degradation values are given in Table 3. 100% dye degradation under UV light was observed in the presence of NTP25-15 in the time period of 5 h, while only 62, 68, 84 and75% degradation was observed with P25, NTP25-04, NTP25-10 and NTP25-20 catalyst respectively. It is noteworthy that complete degradation takes place with NTP25-15 under solar irradiation within the time period of 90 min. This catalyst showed highest efficiency compared to all the other catalysts. The enhanced activity of NTP25-15 under UV/solar light was attributed to the synergistic effect observed in the two phase solid material. It is well known that, this pair of polymorphs can effectively reduce the recombination of photogenerated charge carriers to enhance the photocatalytic activity [19,44,45]. Under UV excitation, anatase in the mixed phase gets activated as it is a good absorber of UV light
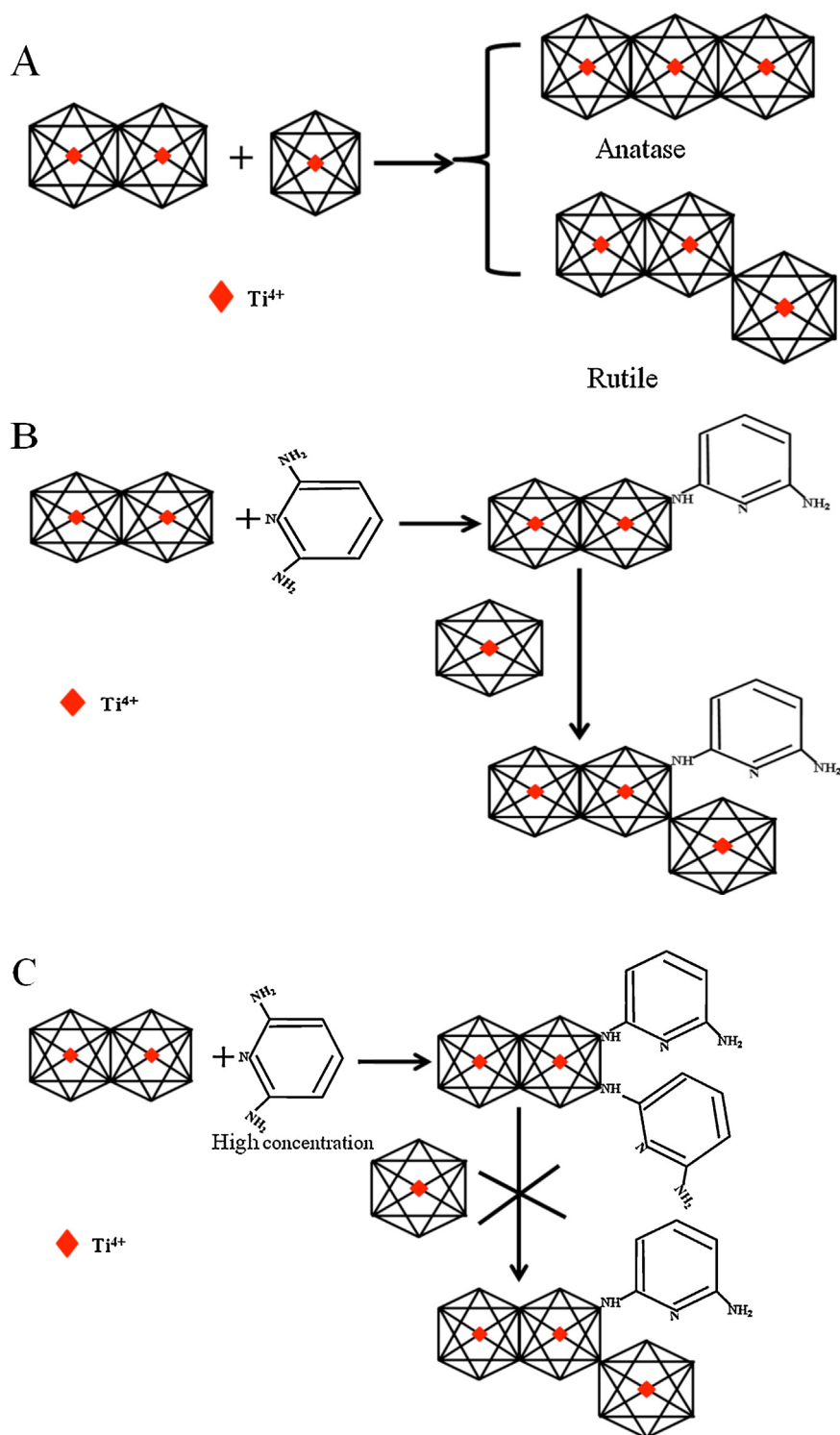
Scheme 1. Mechanism proposed for the formation of anatase and rutile phases in NTP25 samples; (A) the orientation of the TiO_6^{2-} octahedron determines the phase formation of anatase or rutile, (B) interaction of —NH group of DAP with TiO_6^{2-} octahedron and formation of rutile phase at lower concentration of DAP and (C) interaction of two —NH groups of DAP molecule with TiO_6^{2-} octahedron and inhibition of rutile phase formation at higher DAP concentration.

photons as shown in the Scheme 2(i). Further transfer of electrons takes place from the conduction band edge of anatase to the trapping sites of rutile. Thus, rutile serves as a passive electron sink, hindering the recombination in the anatase phase and the hole originating from the anatase transfer to the surface, which accounts
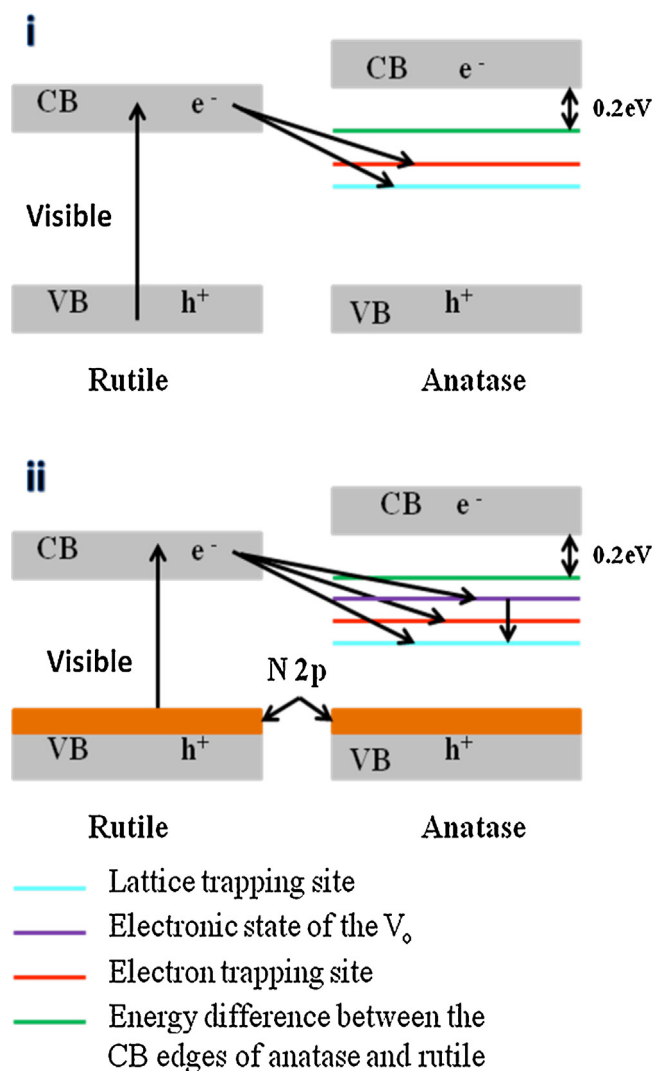
for the enhanced activity of P25 [19,20,46,47]. Similar mechanism takes place even in the case of NTP25-15 under UV irradiation as shown in Scheme 2(ii). Substitutional anion doping with valence higher than the O^{2-} and with a larger ionic size would induce oxygen vacancies at the surface of anatase crystallites, favoring the
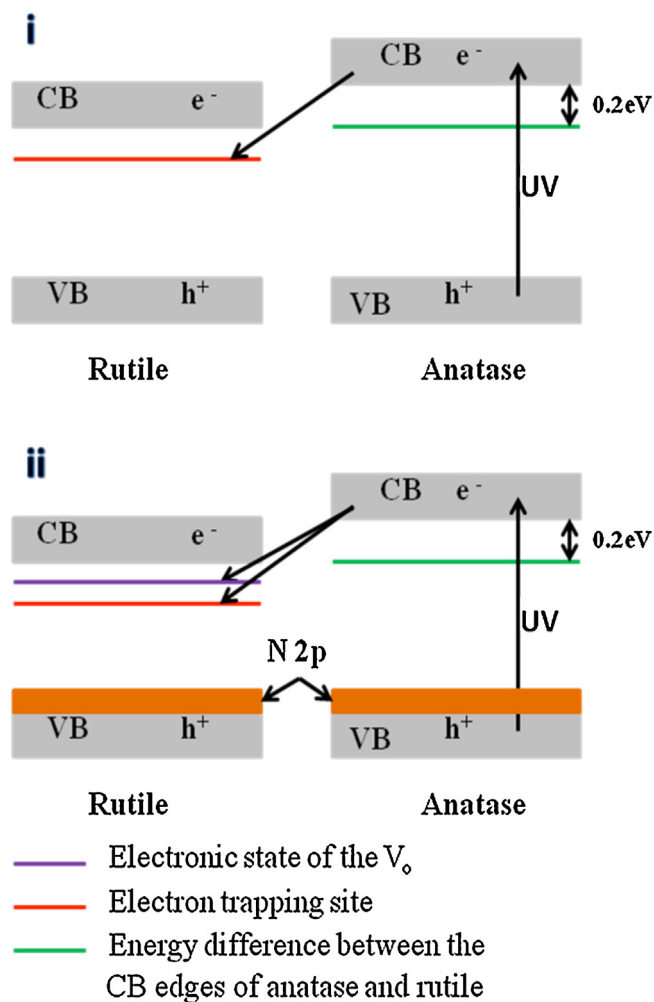
Scheme 2. Charge transfer mechanism in the mixed phase titania under UV light irradiation. (i) P25 (as per Refs. [19,20,46]), (ii) NTP25-15.

Scheme 3. Charge transfer mechanism in mixed phase titania under solar light irradiation. (i) P25 (as per Refs. [19,20,48]), (ii) NTP25-15.

bond rupture leading to the ionic and structural reorganization for the formation of rutile phase. Further the electrical imbalance caused by the incorporated dopant is neutralized by the creation of new oxygen vacancies (which are referred to as induced oxygen vacancies).

In comparison to P25, NTP25-15 possesses higher number of oxygen vacancies to balance the charge neutrality. This additional $(Ti^{3+}-V_o)$ defect level is located around 0.2 eV below the conduction band edge of anatase, which is even lower than the conduction band edge of rutile itself and this level is more prominent in charge transfer reactions. Hence, subsequent electron transfer from the anatase CB to the defect level further favors the charge separation, which might account for the higher activity of NTP25-15 under UV light. The band gap of rutile is more favorable for visible light excitation as the conduction band edge of rutile is 0.2 eV below the conduction band edge of anatase as shown in Scheme 3(i). Under solar excitation, rutile in the mixed phase gets activated as it is a good absorber of solar light photons. In the case of P25 transfer of electrons takes place from the conduction band edge of rutile to the trapping sites of anatase to a lesser extent under solar light. A similar mechanism takes place in the case of NTP25-15 under solar light irradiation as shown in the Scheme 3(ii). In comparison to P25, NTP25-15 possesses two additional defect levels corresponding to $Ti^{3+}-V_o$ and nitrogen dopant. The $Ti^{3+}-V_o$ defect level is below the conduction band edge of anatase, which is even lower than the conduction band edge of rutile itself. Hence subsequent

electron transfer from rutile trapping site to the defect level is favored. Higher activity of NTP25-15 could be accounted to this charge separation [48]. The lattice trapping sites of anatase has energy less than the conduction band edge of rutile [49]. Thus by competing with the recombination, the charge separation activates the catalyst. The hole originating from the rutile valence band participates in the oxidative degradation of organic pollutants. The transfer of electron from rutile to anatase has an activation energy barrier of 8.3×10^{-4} eV based on the measured rate of electron transfer [50]. Due to the low activation barrier, the effective inter particle electron transfer between the two polymorphs is quite possible only when they are in close proximity with similar crystallite sizes [19,20]. The intimate contact between the two polymorphs depends mainly on their crystallite size. Hong et al. had accounted the lower photocatlytic performance of mixed phase titania was due to the larger rutile crystallite size [50].

P25 has anatase to rutile ratio of 82:18 with rutile crystallite size being 85.59 nm, larger than anatase crystallite size (25.56 nm). The sample NTP25-15 has anatase to rutile ratio of 77:23 and the crystallite sizes are in the ratio of 42.4:56.9 nm for the two the phases. Since the crystallite sizes of both the phases is almost same, it can be concluded that both the polymorphs are in intimate contact in NTP25-15 compared to all the other catalysts resulting in
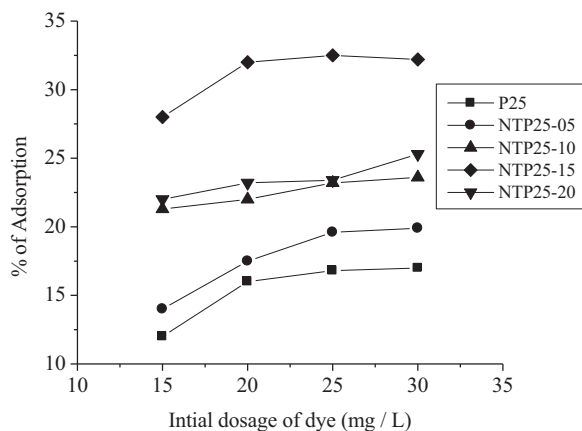
Fig. 8. Plot of percentage of adsorption versus initial concentration of MB on different photocatalyst surface.

lower recombination of charge carriers and thereby accelerating the interfacial charge transfer process.

3.9. Adsorption kinetics

The effect of adsorption of dye on the surface of P25 and NTP25 catalysts were studied at various initial concentrations (C = 15, 20, 25 and 30 mg/L). The results showed that with increase in the dye concentration, the percentage of adsorption increases as shown in Fig. 8. The extent of adsorption on various catalysts shows the following order: NT P25-15 > NT P25-20 > NT P25-10 > NT P25-05 > P25. The maximum extent of adsorption takes place on the surface of NTP25-15 and least for P25.

The obtained adsorption values were tested for different adsorption isotherms. This analysis is important to develop equations to represent results which can be used for designing the waste water treatment system. The isotherm which is frequently studied for adsorption process is Langmuir-Hinshelwood mechanism. Since the extent of adsorption increased with the increase in the dye concentration, a test for Freundilch adsorption isotherm was done. The Freundlich equation is often used for heterogeneous surfaces and term q_e strictly refers to the extent of adsorption and it is given by:

$$q_e = k_f C_e^{1/n} \qquad (4)$$

The linear form of the above equation can be written as

$$\log q_e = \log k_f + \frac{1}{n} \log C_e \qquad (5)$$

where C_e is the equilibrium concentration (mg/L) and $q_e = x/m$, x is the amount of adsorbate and m is the amount of adsorbent at equilibrium and k_f and n are Freundlich constants. n gives an indication of the favorability (n is usually less than unity) and k_f is the capacity of the adsorbent. The plot of $\log q_e$ versus $\log C_e$ is shown in Fig. 9. The intercept and slope gives the values of $\log k_f$ and $1/n$ values (Table 4).

Langmuir isotherm governs the monolayer coverage on the surface containing a finite number of identical sites and this model assumes uniform energies of adsorption and no transmigration of

Table 4

k_f and n values from the plot of $\log C_e$ versus $\log q_e$ (Freundlich isotherm) for the adsorption of MB on the surface of NTP25-15 calculated using Eq. (5).

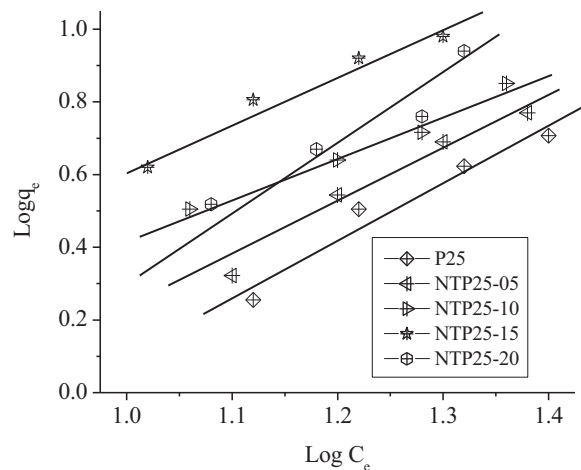| Adsorbent dose (mg/L)	k_f	$1/n$
15	7.413	3.84
20	11.22	1.52
25	10	4.0
30	11.48	3.03

Fig. 9. Plot of $\log q_e$ versus $\log C_e$ for the adsorption of MB on different photocatalysts.

adsorbent takes place. It was experimentally tested and proved that the characteristics of adsorption follow Langmuir adsorption isotherm at all given concentrations. The results could be analyzed in the following way: The initial rise in the adsorption with the concentration of the dye is probably due the higher driving force, larger surface area and smaller size of the dye molecule. The rate of adsorption increases but it may still form unimolecular layer as observed in the Langmuir adsorption isotherm. It is found that Freundlich equation has limitation and it is valid over the concentration range mentioned in the Fig. 8. Above 30 mg/L saturation in adsorption is observed implying the Langmuir characteristics. Therefore at concentrations below 30 mg/L the amount adsorbed becomes proportional to the concentration and resembles Freundlich isotherm, whereas at high concentration a limiting value for adsorption is observed and follows Langmuir adsorption isotherm.

4. Conclusion

Nitrogen doped Degussa P25 TiO$_2$ photocatalyst with two phase solid material of anatase and rutile was prepared using DAP as the nitrogen source. The phase content in the powders could be monitored precisely by varying the DAP concentration. The orientation of the third TiO$_6{}^{2-}$ octahedron plays a very important role in the formation of rutile and anatase phase contents. The catalyst NTP25-15 containing 77% of anatase showed the highest photocatalytic activity for photodegradation of MB, which can be accounted to the following factors: (i) the defect states introduced by the nitrogen dopant serves as trap sites for the photogenereated charge carriers, (ii) the effective inter particle electron transfer between the two polymorphs is quite efficient only when they are in close proximity with similar crystallite sizes and it further reduces the recombination of photogenerated charge carriers by accelerating the interfacial charge transfer process, (iii) synergistic effect is observed between anatase and rutile phases under both UV and solar light facilitating efficient photodegradation.

Appendix A. Supplementary data

Supplementary data associated with this article can be found, in the online version, at http://dx.doi.org/10.1016/j.molcata.2013.02.009.

References

 [1] T. Ohno, K. Sarukawa, K. Tokieda, M. Matsumura, J. Catal. 203 (2001) 82–86.
 [2] A. Hagfeldt, M. Gratzel, Acc. Chem. Res. 33 (2000) 269–277.
 [3] N. Serpone, Res. Chem. Intermed. 20 (1994) 953–992.
 [4] M. Fox, M.T. Dulay, Chem. Rev. 93 (1993) 341–357.
 [5] R.G. Aditi, B.F. Julio, J. Mol. Catal.: A: Chem. 226 (2005) 171–177.
 [6] W. Chiron, A. Fernandes-Alba, A. Rodriguez, E. Garcia-Calvo, Water Res. 34 (2000) 366–377.
 [7] M.A. Anderson, Stud. Surf. Sci. Catal. 103 (1997) 445–461.
 [8] C.M. Schmidt, E. Weitz, Langmuir 23 (2006) 9642–9650.
 [9] D. Gumy, C. Morais, P. Bowen, C. Pulgarin, S. Giraldo, R. Hajdu, J. Kiwi, Appl. Catal. B: Environ. 63 (2006) 76–84.
[10] (a) B. Ohtani, O.O. Prieto-Mahaney, D. Li, R. Abe, J. Photochem. Photobiol. A: Chem. 216 (2010) 179–182;
     (b) U. Stafford, K.A. Gray, P.V. Kamat, A. Varma, Chem. Phys. Lett. 205 (1993) 55–61.
[11] G. Riegel, J.R. Bolton, J. Phys. Chem. 99 (1995) 4215–4225.
[12] G. Liu, F. Li, Z. Chen, G. Qing Lu, H.M. Cheng, J. Solid State Chem. 179 (2006) 331–335.
[13] X. Pan, X. Ma, J. Solid State Chem. 177 (2004) 4098–4103.
[14] S. Yin, H. Yamaki, M. Komatsu, Q. Zhang, J. Wang, Q. Tang, F. Saito, T. Sato, J. Mater. Chem. 13 (2003) 2996–3001.
[15] I-C. Kang, Q. Zhang, J. Kano, S. Yin, T. Sato, F. Saito, J. Photochem. Photobiol. A: Chem. 189 (2007) 232–238.
[16] A.L. Linsebigler, G.Q. Lu, J.J.T. Yates, Chem. Rev. 95 (1995) 735–758.
[17] Y. Li, N.-H. Lee, E.-G. Lee, J.S. Song, S.-J. Kim, Chem. Phys. Lett. 389 (2004) 124–128.
[18] Q.J. Yang, C. Xie, Z.L. Xu, Z.M. Gao, Y.G. Du, J. Phys. Chem. B 109 (2005) 5554–5560.
[19] L.G. Devi, N. Kottam, S.G. Kumar, J. Phys. Chem. C 113 (2009) 15593–15601.
[20] L.G. Devi, N. Kottam, S.G. Kumar, K.S. Anantharaju, Catal. Lett. 131 (2009) 612–617.
[21] G. Liu, Z. Chen, C. Dong, Y. Zhao, F. Li, G.Q. Lu, H.-M. Cheng, J. Phys. Chem. B 110 (2006) 20823–20828.
[22] R.A. Spurr, H. Myers, Anal. Chem. 29 (1957) 760–765.
[23] Y. Wanga, Y. Huanga, W. Hob, L. Zhanga, Z. Zouc, S. Leeb, J. Hazard. Mater. 169 (2009) 77–87.
[24] (a) H. Sun, Y. Bai, H. Liu, W. Jin, N. Xu, J. Photochem. Photobiol. A: Chem. 201 (2009) 15–22;
     (b) J. Yang, J.M.F. Ferreira, Mater. Lett. 36 (1998) 320–324.
[25] X. Yang, C. Cao, L. Erickson, K. Hohn, R. Maghirang, K. Klabunde, Appl. Catal. B: Environ. 91 (2009) 657–662.
[26] K.M. Parida, B. Naik, J. Colloid Interface Sci. 333 (2009) 269–276.
[27] Y. Li, C. Xie, S. Peng, G. Lu, S. Li, J. Mol. Catal.: A: Chem. 282 (2008) 117–123.
[28] Q. Xiang, J. Yu, B. Cheng, H.C. Ong, J. Chem. Asian 5 (2010) 1466–1474.
[29] J. Yu, G. Dai, B. Huang, J. Phys. Chem. C 113 (2009) 16394–16401.
[30] L. Lin, R.Y. Zheng, J.L. Xie, Y.X. Zhu, Y.C. Xie, Appl. Catal. B: Environ. 76 (2007) 196–202.
[31] (a) L. Miao, S. Tanemura, H. Watanable, Y. Mori, K. Kameka, S. Toh, J. Cryst. Growth 260 (2004) 118–124;
     (b) T.C. Jagadale, S.P. Takale, R.S. Sonawane, H.M. Joshi, S.I. Patil, B.B. Kale, S.B. Ogale, J. Phys. Chem. C 112 (2008) 14595–14602.
[32] C.D. Wangner, Anal. Chem. 44 (1972) 1050–1053.
[33] S. Liu, X. Chen, X. Chen, Chin. J. Catal. 27 (2006) 697–702.
[34] T. Matsumoto, N. Iyi, Y. Kaneko, K. Kitamura, S. Ishihara, Y. Takasu, Y. Murakami, Catal. Today 120 (2007) 226–232.
[35] M.E. Jacox, W.E. Thompson, J. Mol. Spectrosc. 228 (2004) 414–431.
[36] T. Ihara, M. Miyoshi, Y. Iriyama, O. Matsumoto, S. Sugihara, Appl. Catal. B: Environ. 42 (2003) 403–409.
[37] K. Fujihara, S. Izumi, T. Ohno, M. Matsumura, J. Photochem. Photobiol. A 132 (2000) 99–104.
[38] K. Suzuki, G. Bley, U. Neukirch, J. Gutowski, N. Takojima, T. Sawada, K. Imai, Solid State Commun. 105 (1998) 571–575.
[39] B. Enright, D. Fitzmaurice, J. Phys. Chem. 100 (1996) 1027–1035.
[40] M. Gopal, W.J.M. Chan, L.C. De Jonghe, J. Mater. Sci. 32 (1997) 6001–6008.
[41] A. Fahmi, C. Minot, P. Fourre, P. Nortier, Surf. Sci. 343 (1995) 261–272.
[42] R.L. Penn, J.F. Banfield, Am. Mineral. 84 (1999) 871–876.
[43] Y. Li, T.J. White, S.H. Lim, J. Solid State Chem. 177 (2004) 1372–1381.
[44] S.B. Park, K.Y. Jung, H.D. Jang, Catal. Commun. 5 (2004) 491–497.
[45] Y. Bessekhouad, D. Robert, J.V. Weber, J. Photochem. Photobiol. A: Chem. 157 (2003) 47–53.
[46] R.I. Bickley, T.G. Carreno, J.S. Lees, L. Palmisano, R.J.D. Tilley, J. Solid State Chem. 92 (1991) 178–186.
[47] A.K. Datye, G. Riegel, G.R. Bolton, M. Huang, M.R. Prairie, J. Solid State Chem. 115 (1995) 236–239.
[48] D.C. Hurum, A.G. Agrios, K.A. Gray, T. Rajh, M.C. Thurnauer, J. Phys. Chem. 107 (2003) 4545–4549.
[49] S. Leytner, J.T. Hupp, Chem. Phys. Lett. 330 (2000) 231–236.
[50] X. Hong, Z. Wang, W. Cai, F. Lu, J. Zhang, Y. Yang, N. Ma, Y. Lin, Chem. Mater. 17 (2005) 1548–1552.